Environmental Science: Atmospheres

ROYAL SOCIETY OF CHEMISTRY

PAPER

View Article Online
View Journal | View Issue



Cite this: *Environ. Sci.: Atmos.*, 2023, **3**, 422

# High efficiency of nitric acid controls in alleviating particulate nitrate in livestock and urban areas in South Korea†

Haeri Kim,[a] Junsu Park,[a] Seunggi Kim,[a] Komal Narayan Pawar[a] and Mijung Song *[ab]

Remarkably, enhanced particulate nitrate ($NO_3^-$) concentrations occur in many environments during particulate matter (PM) pollution; however, information on the formation mechanism and alleviation strategies is still limited. Herein, to explore the $NO_3^-$ formation mechanism and conditions, we measured the concentrations of water-soluble inorganic ions in $PM_{1.0}$ as well as the inorganic gas concentrations of $HNO_3$, $NO_2$, and $NH_3$ in Gimje, a highly dense livestock area, from June to July 2020 and January to February 2021. At the monitoring site, extremely high atmospheric $NH_3$ was measured with an hourly average of 96.9 ± 48.1 ppb, and the daily average of $HNO_3$ and $PM_{1.0}$ was 0.7 ± 0.7 ppb, and 20.1 ± 8.8 μg $m^{-3}$, respectively. A clear increase in the $NO_3^-$ concentration in $PM_{1.0}$ was observed on high pollution days ($PM_{1.0}$ ≥ 20 μg $m^{-3}$), suggesting that $HNO_3$ and $NH_3$ contributed to $NO_3^-$ formation. Moreover, we applied the thermodynamic model ISORROPIA-II to predict the $NO_3^-$ response to the reduction of total $HNO_3$ (TN), total $NH_3$ (TA), and $SO_4^{2-}$. The results showed that controlling TN could be more effective in alleviating particulate $NO_3^-$ than controlling $SO_4^{2-}$ and TA in the livestock area. We also compared this result to that of a nearby urban area, Jeonju. A similar result was observed, with efficient $HNO_3$ control, which reduced the $NO_3^-$ concentration in Jeonju. These measurements and simulations indicated that $NO_x$ control could be the most effective approach to reduce particulate $NO_3^-$ concentrations in both livestock and urban areas. Our results provide a significant contribution to developing a strategy for alleviating particulate $NO_3^-$ pollution.

Received 10th May 2022
Accepted 26th December 2022

DOI: 10.1039/d2ea00051b

rsc.li/esatmospheres



### Environmental significance

The particulate nitrate ($NO_3^-$) concentration is often enhanced during particulate matter (PM) pollution; however, there is limited information on the formation mechanism and reduction strategies of particulate $NO_3^-$. Using thermodynamic model ISORROPIA-II and the measurements of inorganic gaseous species and water-soluble ions of $PM_{1.0}$, we show that controlling total nitrate could be more effective in reducing particulate $NO_3^-$ and PM concentrations than controlling $SO_4^{2-}$ and total ammonia in a livestock area. Moreover, a similar result was observed with efficient $HNO_3$ control, which reduced $NO_3^-$ and PM concentrations in a nearby urban area. This suggests that $NO_x$ control is an effective approach to reduce particulate $NO_3^-$ in both livestock and urban areas. In the future, a strategy can be developed to reduce $NO_3^-$ pollution by using the results of this study.

## Introduction

Particulate matter (PM) below 2.5 μm in aerodynamic diameter ($PM_{2.5}$) significantly impacts the air quality, global climate, and human health.[1–3] $PM_{2.5}$ is emitted directly into the atmosphere. $PM_{2.5}$ mainly contains ammonium sulfate ($(NH_4)_2SO_4$), ammonium nitrate ($NH_4NO_3$), and organic aerosols formed *via* photochemical reactions of precursor gaseous species such as nitrogen oxides ($NO_x$), ammonia ($NH_3$), sulfur dioxide ($SO_2$), and volatile organic compounds.[4] In $PM_{2.5}$, secondary inorganic aerosols (SIAs) account for more than 80% by mass, depending on the location and season.[5,6]

Among SIAs, the concentration of $NH_4NO_3$ remarkably increases during $PM_{2.5}$ pollution in various environments.[7–9] $NH_4NO_3$ can be produced by a series of chemical reactions of $NO_x$ and $NH_3$, as follows:[4]

$$NO_2\ (g) + OH\ (g) \rightarrow HNO_3\ (g) \quad (R1)$$

$$NH_3\ (g) + HNO_3\ (g) \rightarrow NH_4NO_3\ (s, aq) \quad (R2)$$

In the atmosphere, nitrogen dioxide ($NO_2$) reacts with hydroxyl radicals (OH) to produce nitric acid ($HNO_3$). $HNO_3$

[a]*Department of Environment and Energy, Jeonbuk National University, Jeonju 54896, Korea*

[b]*Department of Earth and Environmental Sciences, Jeonbuk National University, Jeonju 54896, Korea*

† Electronic supplementary information (ESI) available. See DOI: https://doi.org/10.1039/d2ea00051b

then reacts with $NH_3$ to form $NH_4NO_3$. $NH_4NO_3$ is a semi-volatile species that can partition primarily from the gas-phase to the particle-phase, depending on the temperature.[4]

Studies on night-time chemistry have addressed nitrate ($NO_3^-$) formation by heterogeneous reactions.[10] During night-time, nitrogen trioxide ($NO_3$) is produced by the reaction of $NO_2$ and ozone ($O_3$) (R3), and the $NO_3$ reacts with $NO_2$ to form dinitrogen pentoxide ($N_2O_5$) (R4). Heterogeneous uptake of $N_2O_5$ on aerosol surfaces produces $HNO_3$ *via* hydrolysis (R5).[4]

$$NO_2\ (g) + O_3\ (g) \rightarrow NO_3\ (g) + O_2\ (g) \quad (R3)$$

$$NO_3\ (g) + NO_2\ (g) \rightarrow N_2O_5\ (g) \quad (R4)$$

$$N_2O_5\ (g) + H_2O\ (l) \rightarrow 2HNO_3\ (aq) \quad (R5)$$

These reactions produce particulate $NO_3^-$ under $NH_3$-rich conditions.[4] However, under $NH_3$-poor conditions, $HNO_3$ can be formed through the reaction of other alkaline species.[11]

$NO_x$ and $NH_3$, the main precursor gases of $NH_4NO_3$, are emitted into the atmosphere by various sources. $NO_x$ is emitted not only by anthropogenic activities such as combustion of oil and coal, energy generation, on-road transportation, and agricultural activities, but also by natural sources such as soil, biomass burning, and lightning.[12,13] In California[14] and the North China Plain,[15] where there are active agricultural areas, the total $NO_x$ emissions accounted for more than 30% in 2013 and 50% in 2017. $NH_3$ is mainly emitted from agricultural sources, such as fertilizer application, soil, and livestock, accounting for approximately 90% of the total global $NH_3$ emission,[12,16] which has dramatically increased by 80% from 1970 to 2017.[12]

Studies have been conducted to understand the formation mechanism and develop effective reduction strategies for $NH_4NO_3$ pollution. Some modeling studies have suggested that reduction of total $NH_3$ (TA) could be the most effective method to reduce PM concentrations.[9,17] For instance, Franchin *et al.* (2018) used ISORROPIA-II modeling showing that a reduction in the $NH_3$ concentration by approximately 50% could decrease the $PM_{1.0}$ concentration by ~36% in a rural area in Utah, United States. Moreover, in central China, which is surrounded by rural and urban areas, GEOS-Chem modeling results showed that a reduction in $NH_3$ emissions by 47% reduced the $PM_{2.5}$ concentrations by ~9% in July and ~11% in January.[17] By contrast, other modeling studies have shown that reducing $NO_x$ emissions would be more effective than reducing $NH_3$ emissions for controlling PM.[18–20] Guo *et al.* (2018) showed that controlling $NO_x$ emission would effectively reduce $NO_3^-$ concentrations in an agricultural area in Cabauw, Netherlands. Furthermore, Chen *et al.* (2014) suggested that a 50% reduction in $NO_x$ emissions would decrease $PM_{2.5}$ and $NO_3^-$ concentrations by more than 24% and 42%, respectively, in an urban area in Bakersfield, USA. Analysis of ground-based data showed that $NH_4NO_3$ formation in the Salt Lake Valley is likely to be total $HNO_3$ (TN)-limited, and, thus, reduction of $NO_x$ is effective in improving the air quality.[20] However, scientific data on highly efficient control strategies of precursor gas in alleviating particulate $NO_3^-$ in different areas are still lacking.

In this study, to determine $NH_4NO_3$ formation and related PM pollution conditions, two intensive field measurements of $NH_3$, $NO_2$, $HNO_3$, and water-soluble inorganic ions (WSIIs) in $PM_{1.0}$ were performed in the summer in Gimje, a rural area in South Korea. Gimje is a highly dense livestock area with populated livestock facilities and farms.[21] Extremely high $NH_3$ emission[22] and PM pollution[23] have been reported in this region. There are almost no studies on the temporal distribution of WSIIs and their precursor gases. In this study, the WSIIs and inorganic gas-particle-phase partitioning of $NH_4NO_3$ were analyzed by exploring the WSIIs and inorganic gases. Based on the measurement dataset and thermodynamic model ISORROPIA-II, we discuss the effective implementation of PM and $NO_3^-$ reduction strategies in livestock-dense areas. Moreover, we compared the results acquired from the rural area with those from a nearby urban area, Jeonju, *via* thermodynamic modeling by using the $NH_3$ and WSII concentrations in $PM_{2.5}$ data measured from May 2019 to April 2020 by Park *et al.* (2021).[8]

# Methods

### Measurements

Particulate WSIIs and inorganic gases were measured in Gimje, Jeollabuk-do, South Korea (35.8395° N, 126.9889° E) (Fig. 1). The monitoring site has livestock complexes for raising pigs and chickens and large-scale farms with open manure storage facilities,[21,24] resulting in high $NH_3$ emissions.[22]

Two intensive field measurements were performed during the summer (June to July 2020) and winter (January to February 2021). In the livestock area, concentrations of inorganic gases such as $NH_3$, $NO_x$ (NO, and $NO_2$), and $HNO_3$, and WSIIs in $PM_{1.0}$ ($Na^+$, $NH_4^+$, $Mg^{2+}$, $Ca^{2+}$, $K^+$, $NO_3^-$, $SO_4^{2-}$, and $Cl^-$) were measured. Atmospheric $NH_3$ was measured every 1 s using a real-time $NH_3$ instrument (DLT-100, Los Gatos Research, USA) using off-axis integrated cavity output spectroscopy. In principle, the $NH_3$ instrument using specific wavelengths does not require external calibration.[25] However, we performed calibration to confirm the performance of the instrument by mixing standard $NH_3$ (9.2 ppm, with an accuracy of ±2%, Air Korea, Korea) and $N_2$ (99.999%, Air Korea, Korea) gases before and after field measurements, resulting in an $R^2$ of 0.9999 (Fig. S1†). The detailed procedure for the calibration and measurement of atmospheric $NH_3$ is described by Park *et al.* (2021). For the analysis, we used hourly averaged concentrations of atmospheric $NH_3$. The $NO_x$ concentration was also monitored every 1 m using a $NO_x$ instrument (Serinus 40 Oxides of Nitrogen, Ecotech, Australia), based on the chemiluminescence method. Before and after conducting the field measurements, calibration was conducted by mixing standard NO (4.9 ppm, with an accuracy of ±10%, Air Korea, Korea) and $N_2$ (99.999%, Air Korea, Korea) gases at four different concentrations (20, 15, 12, and 0 ppb), which resulted in an error concentration of ~3%. The hourly averaged concentration of atmospheric $NO_x$ was used for the analysis.

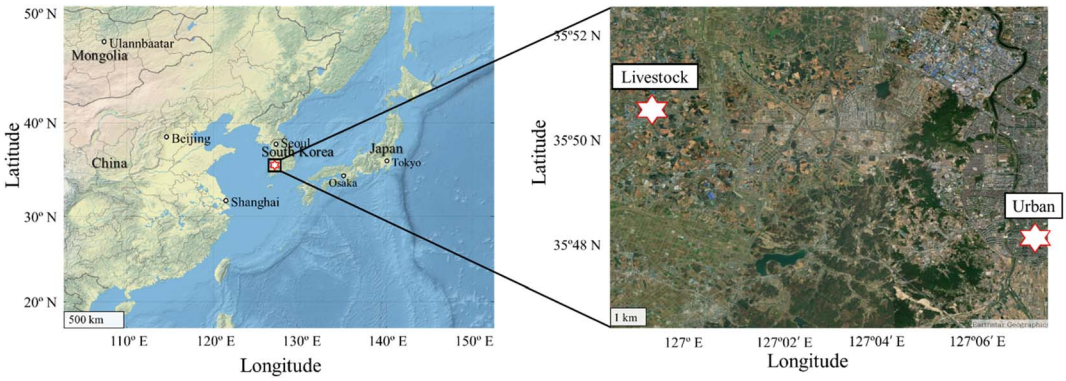


Fig. 1 Map of the measurement site in livestock and urban areas, Jeollabuk-do, South Korea.

$PM_{1.0}$ and $HNO_3$ were collected using a two-stage sequential air sampler (APM Engineering, PMS-114, Korea) which has been widely used.[26,27] The sequential air sampler consisted of two stages for collection of $PM_{1.0}$ on a Teflon filter (PTFE, 66155, PALL, USA) at the first stage, and of $HNO_3$ on a nylon filter (Nylon, 1213776, GVS, USA) at the second stage. It was operated at a flow rate of 16.7 L $min^{-1}$ for 24 h from 00:00 am to 00:00 am the following day during the measurement period. During the sampling, some semi-volatile species (*i.e.* $NO_3^-$, $NH_4^+$ and $HNO_3$) could be evaporated, leaving approximately ~10% of their total mass on the filters.[28,29] A total of 84 samples for $PM_{1.0}$ (42 samples) and $HNO_3$ (42 samples) were collected during all measurements. Subsequently, all filter samples were stored at −4 °C in a freezer and then analyzed within two weeks after collection. The $PM_{1.0}$ mass concentration collected from the Teflon filter was observed based on the procedure of the method of the USA Environmental Protection Agency.[30] To analyze the $HNO_3$ and WSIIs of $PM_{1.0}$, each filter sample was extracted in purified water (18.2 MΩ cm, Merck Milli-Q®, Millipore, Burlington, MA, USA). A detailed extraction procedure was described previously.[31] The extracts from nylon filters were analyzed to quantify the concentration of $HNO_3$, and the extracts from Teflon filters were analyzed to determine five cations ($Na^+$, $NH_4^+$, $Mg^{2+}$, $Ca^{2+}$, and $K^+$) and three anions ($NO_3^-$, $SO_4^{2-}$, and $Cl^-$) using ion chromatography (Aquion, Thermo Scientific, USA). The method detection limits (MDLs) of $Na^+$, $NH_4^+$, $Ca^{2+}$, $Mg^{2+}$, $K^+$, $NO_3^-$, $SO_4^{2-}$, and $Cl^-$ were 0.01, 0.01, 0.03, 0.01, 0.02, 0.02, 0.03 and 0.02 μg $m^{-3}$, respectively. For gaseous species, the MDLs of $HNO_3$, $NO_x$, and $NH_3$ were 0.01, 0.4,[32] and 0.5 (ref. 25) ppb, respectively. Hourly averaged meteorological parameters, including relative humidity (RH), temperature, wind direction, precipitation, and wind speed, were obtained during the measurement period from the Korea Meteorological Administration in Jeonju.[33]

### Thermodynamic modeling

To estimate whether $HNO_3$ or $NH_3$ is the limiting factor for particulate $NO_3^-$ formation and to calculate aerosol liquid water content (ALWC), we used ISORROPIA-II, an extensively applied thermodynamic equilibrium model based on a $Na^+$–$Cl^-$–$Ca^{2+}$–$K^+$–$Mg^{2+}$–$SO_4^{2-}$–$NH_4^+$–$NO_3^-$–$H_2O$ aerosol system.[18,34,35] As model inputs, the measured concentrations of TA (particle-phase $NH_4^+$ + gas-phase $NH_3$), TN (particle-phase $NO_3^-$ + gas-phase $HNO_3$), $Na^+$, $K^+$, $Ca^{2+}$, $Mg^{2+}$, $Cl^-$, and $SO_4^{2-}$ and meteorological parameters in the rural area were used. ALWC was also calculated using measured data of inorganic gases, WSIIs, temperature, and RH.[35] It was reported that a correlation coefficient between the simulated ISORROPIA-II ALWC and the measured hygroscopic growth factors agreed well at ~0.89; however, the uncertainty of the predicted ALWC in aerosols would be ~20% compared to the observed ALWC.[36] This underestimation might be due to the unidentified organic species information in ISORROPIA-II.[35,36]

In this study, we used the "forward" mode, which calculates gas-particle equilibrium partitioning concentrations using the total concentration of species because this mode provides substantially better computational results for the concentrations of inorganic gases than the reverse mode.[18,37] The mean RH of 74.7 ± 11.3% observed throughout the monitoring site was below the deliquescence relative humidity (DRH) for pure $(NH_4)_2SO_4$.[4] However, $PM_{1.0}$ could still absorb water below the DRH of the pure salt because PM is a complex mixture of various inorganic salts and organic compounds.[37–39] Therefore, we used the "metastable state" solution, assuming that the aerosol compositions are an aqueous supersaturated solution that prevents the formation of a solid precipitate.[35,37]

To compare the phenomena of gas-particle partitioning between rural and urban areas, we also calculated the limiting factor of particulate $NO_3^-$ formation and gas-particle partitioning using previous data (measured from May 2019 to April 2020) of WSIIs in $PM_{2.5}$ and $NH_3$ measured in Jeonju, an urban area situated approximately 10 km from Gimje.[8] In this study, $HNO_3$ measurement data were unavailable for the urban area; thus, the concentration was estimated using the method of Seo *et al.* (2020).[40] The uncertainty in the estimated TN was confirmed by comparing the measured TN at the rural site (Fig. S2†). To confirm the thermodynamic equilibrium, we also compared the measured and predicted values of the SNA ($SO_4^{2-}$, $NO_3^-$, $NH_4^+$) species (Fig. S1 and S3†). Fig. S3† shows the scatter plots of observations against model predictions of

the major secondary inorganic aerosol (SIA) species ($NH_4^+$, $NO_3^-$ and $SO_4^{2-}$) in livestock and urban areas during measurement periods. A good correlation was found between observations and model predictions, suggesting the good performance of ISORROPIA-II.

### Conditional probability function (CPF) analysis

To identify the potential regional-scale transport and local emission sources, a conditional probability function (CPF) analysis was conducted using the wind direction, wind speed, and $NH_3$ and $NO_2$ concentrations. The CPF estimates a probability that the given source contribution from the given wind speed and wind direction will exceed a threshold criterion. The threshold criterion was set at the 80$^{th}$ percentile to indicate the directionality of the source.

## Results and discussion

### Overview of gaseous species and WSIIs

Two intensive measurements of inorganic gaseous species (namely, $HNO_3$, NO, $NO_2$, and $NH_3$) and WSIIs in $PM_{1.0}$ were conducted in the highly dense livestock area of Gimje during the summer and winter of 2020–2021. Fig. 2 shows the daily averaged variations in meteorological parameters, gaseous species, and WSIIs in $PM_{1.0}$. Over the study period, the daily average temperature was 15.1 ± 9.8 °C, and RH was 74.7 ± 11.3% (Fig. 2A). The mean concentrations of $NH_3$, $HNO_3$, NO, and $NO_2$ were 96.9, 0.7, 2.3, and 21.3 ppb, respectively (Fig. 2B). The atmospheric $NH_3$ concentration in the populated livestock area was significantly (2–35 times) higher than that in other livestock and urban areas listed in Table 1.[8,27,41–45] This is because of livestock activities, open manure storage facilities, and livestock waste disposal in the region. The $HNO_3$ concentration at the monitoring site was lower than that reported in Seoul,[27] Quzhou, Beijing,[41] and New Delhi[42] but higher than that reported in Jeonju,[8] Seolseongmyeon,[27] Gucheng,[43] Niangon Adjamé[44] and San Diego[45] (Table 1).

The daily concentrations of $PM_{1.0}$ and its WSIIs are shown in Fig. 2C. The daily averaged $PM_{1.0}$ mass concentration ranged from 3.3 to 45.2 μg m$^{-3}$, with an average of 20.1 ± 8.8 μg m$^{-3}$. $NO_3^-$, $SO_4^{2-}$, and $NH_4^+$ were the major components of $PM_{1.0}$, and the daily concentration of $NO_3^-$ ranged from 0.4 to 22.0 μg m$^{-3}$ with an average of 4.8 ± 3.9 μg m$^{-3}$. The daily $SO_4^{2-}$ concentrations fluctuated between 0.1 and 7.1 μg m$^{-3}$, with an average of 3.5 ± 1.8 μg m$^{-3}$. The daily $NH_4^+$ concentrations varied from 0.2 to 9.4 μg m$^{-3}$ and showed an average of 2.8 ± 1.6 μg m$^{-3}$. Among all WSII species, a significant dominance of $NO_3^-$ was observed at the livestock site during the measurement period (Fig. 2C).

All WSIIs, $PM_{1.0}$, and inorganic gaseous species, except for $SO_4^{2-}$ and $HNO_3$, exhibited higher concentrations in the winter (Table S1†). Among the WSIIs, the $NO_3^-$concentration was remarkably enhanced from 2.9 μg m$^{-3}$ in the summer to 7.3 μg m$^{-3}$ in the winter (Table S1 and Fig. S4E†). However, the $HNO_3$ concentration dramatically decreased to an average of 0.1 ppb in the winter (summer: 1.1 ppb) (Table S1 and Fig. S4C†). Theoretically, $NH_3$ and $HNO_3$ phases are dependent on temperature and RH.[4] $NH_4NO_3$ partitions can occur from the particle-phase to the gas-phase at low RH and high temperature.[4,46] For this reason, $NO_3^-$ is mostly present in gaseous $HNO_3$ during the summer and has low concentrations, whereas $NO_3^-$ is partitioned into particle-phase $NO_3^-$ during the winter, resulting in higher atmospheric $NO_3^-$ concentrations. Our results, which revealed low $HNO_3$ levels in the summer and high $NO_3^-$ levels in the winter, are consistent with previously reported ones.[27,47] $NH_3$ is generally temperature-dependent. Thus, high $NH_3$ levels have been reported in the summer.[8,27,48] However, the atmospheric $NH_3$

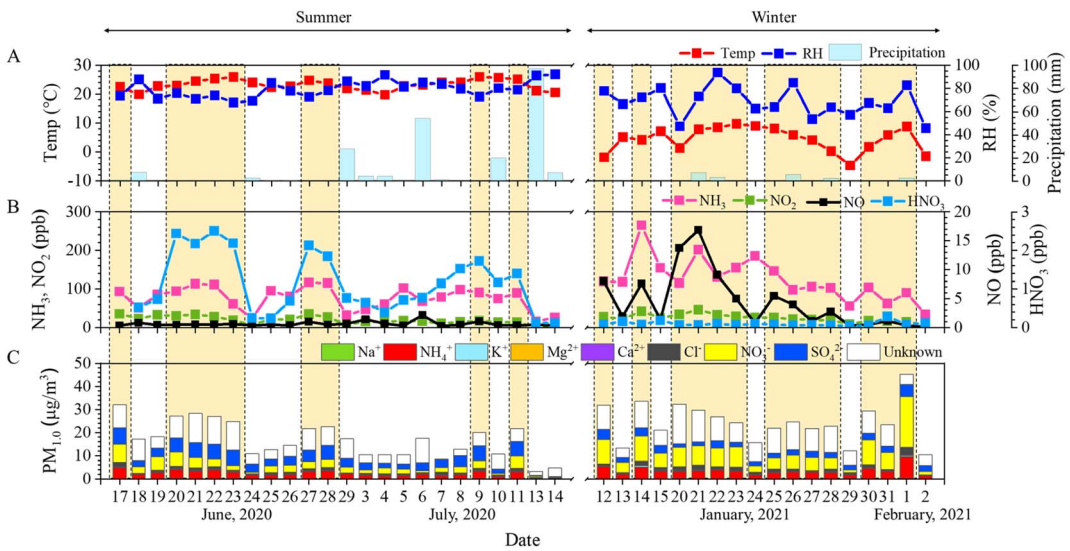


Fig. 2 Daily averaged variations in (A) temperature (temp.), relative humidity (RH), and precipitation, (B) $NH_3$, $NO_2$, NO, and $HNO_3$ concentrations, and (C) water-soluble ions in $PM_{1.0}$ in the livestock area during the measurement period. The light-yellow shadows represent $PM_{1.0}$ pollution days ($PM_{1.0} \geq 20$ μg m$^{-3}$).

Table 1 List of atmospheric average $NH_3$ and $HNO_3$ concentrations in various environments

| Location | Period | $NH_3$ (unit: ppb) | $HNO_3$ (unit: ppb) | References |
|---|---|---|---|---|
| **Livestock area** | | | | |
| Gimje, Korea | 2020.6–2020.7<br>2021.1–2021.2 | 96.9 | 0.7 | This study |
| Seolseongmyeon, Korea | 2009.1–2018.12 | 50.0 | 0.4 | Sung *et al.* (2020)[27] |
| Quzhou, China | 2011.1–2014.12 | 31.2 | 2.7 | Xu *et al.* (2016)[41] |
| Gucheng, China | 2013.5–2013.9 | 36.2 | 0.2 | Meng *et al.* (2018)[43] |
| Niangon Adjamé, Côte d'Ivoire | 2015.12–2016.2 | 44.0 | 0.2 | Bahino *et al.* (2018)[44] |
| **Urban area** | | | | |
| San Diego, United States | 2007.2–2012.3 | 3.3 | 0.2 | Li *et al.* (2014)[45] |
| Seoul, Korea | 2009.1–2018.12 | 7.5 | 0.7 | Sung *et al.* (2020)[27] |
| Beijing, China | 2011.1–2014.12 | 17.2 | 3.2 | Xu *et al.* (2016)[41] |
| New Delhi, India | 2017.12–2018.2 | 33.9 | 1.0 | Acharja *et al.* (2020)[42] |
| Jeonju, Korea | 2019.5–2020.4 | 10.5 | 0.2[a] | Park *et al.* (2021)[8] |

[a] Estimation based on an equation from Seo *et al.*, 2020.

concentration was significantly higher in the winter (124.6 ppb) than in the summer (76.0 ppb) (Table S1 and Fig. S4D†). The plausible reasons for this observation are (1) active manure production at the open storage from the livestock farms and (2) dense $NH_3$ emissions from mechanically ventilated farms with a low ventilation rate in winter in the study area.[31] Higher $NH_3$ concentrations have been reported previously in the winter than in other seasons in livestock areas.[31,49]

## Enhancements of nitrate during PM pollution

To investigate the phenomenon of $PM_{1.0}$ pollution in the livestock area, we compared the chemical characteristics of $PM_{1.0}$ on clean and pollution days. Based on $PM_{1.0}$ mass concentrations, we classified days into clean (daily average $PM_{1.0} < 20$ μg $m^{-3}$) and pollution days (daily average $PM_{1.0} \geq 20$ μg $m^{-3}$), as suggested in previous studies.[50,51] On clean days, the average concentration of $PM_{1.0}$ was 12.1 ± 4.0 μg $m^{-3}$, and WSIIs accounted for 58.2% (7.1 μg $m^{-3}$) of $PM_{1.0}$ (Fig. 3A). $SO_4^{2-}$ was

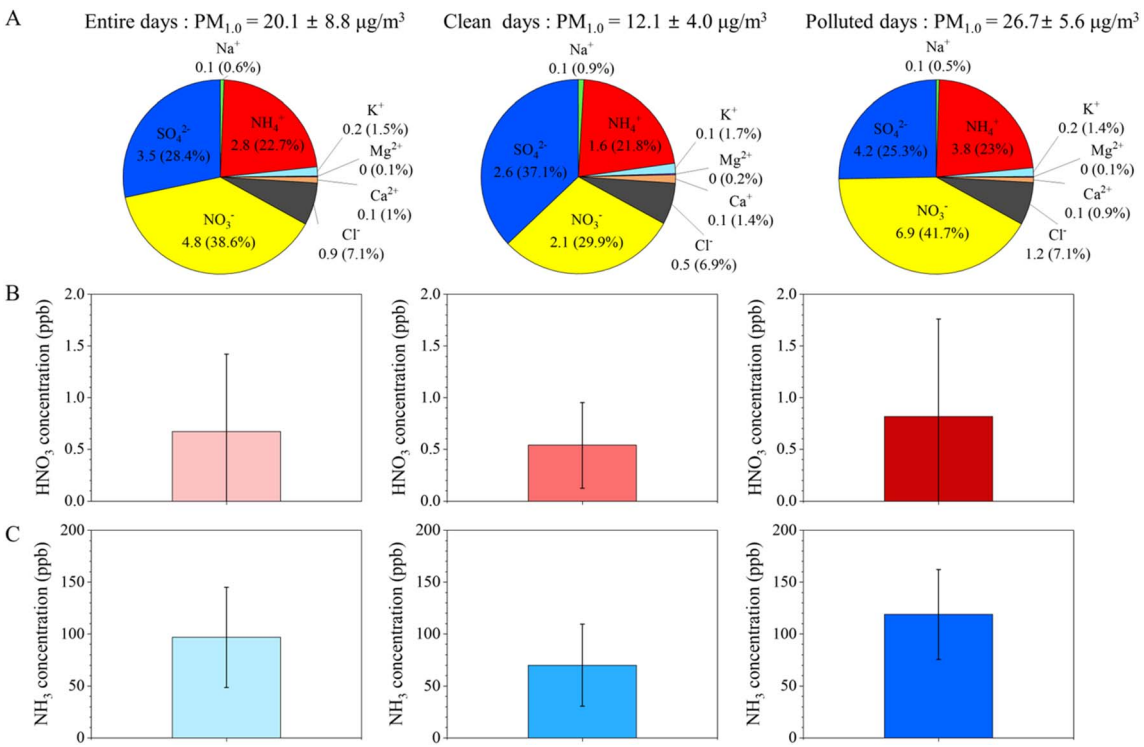


Fig. 3 Comparison of (A) water-soluble ions in $PM_{1.0}$, (B) $HNO_3$ concentration, and (C) $NH_3$ concentrations for entire, clean ($PM_{1.0} < 20$ μg $m^{-3}$), and high pollution ($PM_{1.0} \geq 20$ μg $m^{-3}$) days.

 

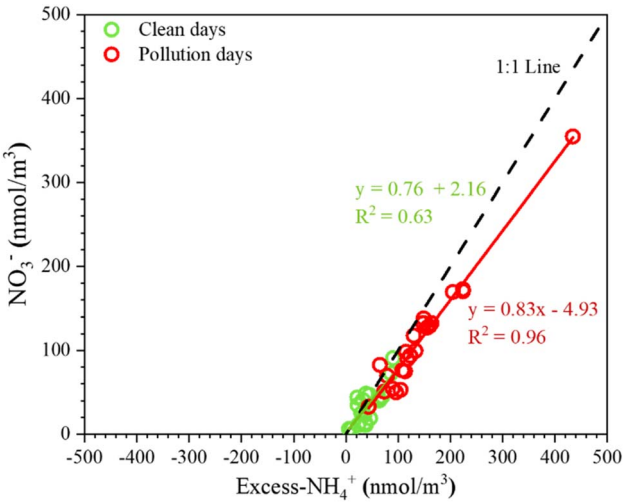


Fig. 4 Scatter plot of molar concentrations of $NO_3^-$ and excess-$NH_4^+$ in the livestock area during clean and pollution days. The green and red lines represent the regression of the clean and pollution days, respectively.

the most dominant ion during the clean days, accounting for 37.1% of $PM_{1.0}$, followed by $NO_3^-$ (29.9%) and $NH_4^+$ (21.8%). Out of 42 days, 23 were defined as $PM_{1.0}$-pollution days at the monitoring site. During pollution days, the daily averaged concentration of $PM_{1.0}$ was 26.7 ± 5.6 μg $m^{-3}$ with a remarkably enhanced $NO_3^-$ fraction (41.7%) in $PM_{1.0}$ (Fig. 3A), followed by $SO_4^{2-}$ (25.3%) and $NH_4^+$ (23.0%). Moreover, the daily average concentrations of $NH_3$ and $HNO_3$ increased significantly to 118.9 ppb and 0.8 ppb, respectively, during pollution days when compared with those during clean days (70.1 ppb and 0.5 ppb, respectively) (Fig. 3B and C). These findings suggest that $NH_3$ and $HNO_3$ play a critical role in $NO_3^-$ formation during high-$PM_{1.0}$ events.

Fig. S5† illustrates the CPF result during pollution days. A high probability of $NH_3$ concentration (179 ppb at the 80$^{th}$ percentile) was observed around the measurement site during pollution days, suggesting that the high levels of $NH_3$ were mostly affected by local sources around the livestock complexes rather than long-range transport.

### $PM_{1.0}$ nitrate formation

Fig. 4 shows the relationship between $NO_3^-$ and excess-$NH_4^+$ molar concentrations. The excess-$NH_4^+$ concentration ranged from 6.0 to 434.3 nmol $m^{-3}$, and $NO_3^-$ molar concentrations increased with excess-$NH_4^+$ molar concentrations during both clean and pollution days, supporting that $NO_3^-$ formation always occurred at the monitoring site. The excess-$NH_4^+$ and $NO_3^-$ molar concentrations showed a significant correlation, with a slope close to 1.0, thereby indicating that the formation of $NH_4NO_3$ was primarily through the reaction between $NH_3$ and $HNO_3$. This is because of the extremely high levels of atmospheric $NH_3$ at the livestock site during the study period.[52] Moreover, a shallower slope for both clean (0.76) and pollution (0.83) days was observed for a livestock site, indicating that most of the measured $PM_{1.0}$ samples were residual $NH_4^+$ associated with species other than $NO_3^-$, such as ammonium chloride ($NH_4Cl$). This implies that there is enough excess $NH_4^+$ that it can drive the partitioning of other semi-volatile acids such as $HNO_3$ and HCl.[53]

### $HNO_3/NH_3$ limitation of particulate nitrate formation

In the livestock area, PM pollution with a drastic enhancement of $NO_3^-$ occurred under $NH_3$-rich conditions, indicating that both $NH_3$ and $HNO_3$ are critical precursors for $PM_{1.0}$ nitrate formation. To suggest a reduction of such high $NO_3^-$ concentrations in the livestock area, we calculated the limiting factor for $NO_3^-$ formation using the ISORROPIA-II model.[35,54] The measurement data of the average WSII concentrations, temperature, and RH were used as the model input data (Table S1†).

Fig. 5A shows the contour plots of simulated $NO_3^-$ concentrations depending on the TA and TN levels at the minimum $SO_4^{2-}$ (~1 μg $m^{-3}$) and maximum $SO_4^{2-}$ (~10 μg $m^{-3}$) concentrations, respectively. In this figure, the left side is the TA-limited area and the right side is the TN-limited area, which were calculated using eqn (1) (unit of each species: μmol $m^{-3}$) as follows:[55]

$$R = \frac{\mathrm{TA}}{2\mathrm{SO_4^{2-}} + \mathrm{NO_3^-} + \mathrm{HNO_3} + \mathrm{Cl^-} + \mathrm{HCl^-} - 2\mathrm{Ca^{2+}} - \mathrm{Na^+} - \mathrm{K^+} - 2\mathrm{Mg^{2+}}} \quad (1)$$

The measurement data of TA and TN during clean (black circles) and pollution days (pink circles) are shown in Fig. 5. All measured data were TN-limited on both clean and pollution days in all cases of minimum and maximum $SO_4^-$ concentrations, given the $NH_3$-rich concentration in the study area (Fig. 5A). $NO_3^-$ formation in livestock can be controlled through $HNO_3$. Hence, to reduce $HNO_3$ concentrations, controlling $NO_x$ emissions might be an important approach to reduce $NO_3^-$ concentrations and thus improve air quality in livestock areas.

Park *et al.* (2021) observed remarkable $NH_4NO_3$ formation during high $PM_{2.5}$ events at nearby urban sites. To compare the results of the limiting factor for $NO_3^-$ formation in an urban area, we calculated the limiting factor in Jeonju, a nearby urban area, using measurement data from May 2019 to April 2020.[8] The method and procedure applied for ISORROPIA-II simulation were used for this step as well. The measurement values of the WSIIs in $PM_{2.5}$, $NH_3$, temperature, and RH in the nearby urban area were used as the input data (Table S1†);[8] however,

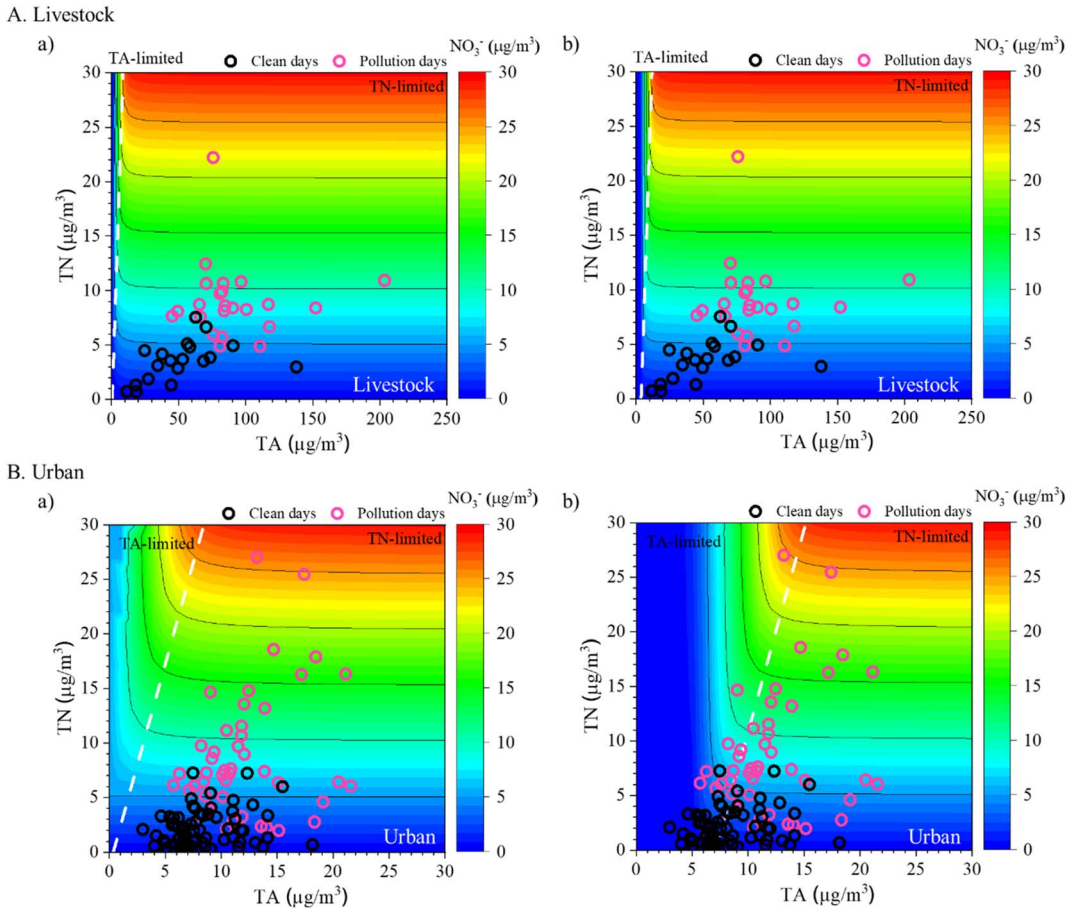


Fig. 5 $NO_3^-$ concentrations calculated using the ISORROPIA-II model depending on total nitrate (TN) and total ammonia (TA) concentrations under (a) $SO_4^{2-} = 1$ μg m$^{-3}$ and (b) $SO_4^{2-} = 10$ μg m$^{-3}$ in the (A) livestock area and under (a) $SO_4^{2-} = 1$ μg m$^{-3}$ and (b) $SO_4^{2-} = 20$ μg m$^{-3}$ in (B) the urban area[8] during clean and pollution days. Measurement data of TN and TA concentrations during the monitoring periods are shown by black circles (clean days) and pink circles (pollution days).

the $HNO_3$ concentration was estimated using ISORROPIA-II because of the absence of data (details are given in S1 in the ESI†). The simulation results showed that under low-$SO_4^{2-}$ conditions (~1 μg m$^{-3}$), all observed data were affected by the TN-limited regime on both clean and pollution days in the urban area (Fig. 5B). In contrast, although under high-$SO_4^{2-}$ (~20 μg m$^{-3}$), the measured data fell into both TA-limited and TN-limited regimes during clean days, and most of the data fell into the TN-limited regime during pollution days (Fig. 5B). As the daily $SO_4^{2-}$ concentration in the urban area was ~4.3 μg m$^{-3}$, the TN-limited regime was more reliable in most cases. This shows that high $NO_3^-$ production in the urban area during $PM_{2.5}$-pollution days was also mainly controlled by $HNO_3$. Therefore, to alleviate particulate $NO_3^-$ in PM in both livestock and nearby urban areas, control of $NO_x$ emissions (which reduces the $HNO_3$ concentration) could be crucial.

### The efficiency of PM reduction *via* precursor controls

To understand the alleviating efficiency of particulate $NO_3^-$ in PM in livestock and urban areas, we performed a sensitivity analysis using ISORROPIA-II, for which the measurement-averaged data were used as input data (Table S1†). Given the abundance of inorganic salts in both areas, we assumed that the $SO_4^{2-}$–$NH_4^+$–$NO_3^-$–$H_2O$ system is in equilibrium and that particulate $NO_3^-$ is formed through the gas-particle partitioning of $NH_3$ and $HNO_3$.

First, we attempted to control the TN concentration to study the decrease in particulate $NO_3^-$ and PM concentrations caused by $HNO_3$ reduction in both livestock and urban areas. In Korea, $HNO_3$ and $NO_x$ are mainly locally contributed rather than long-range transported to form a particle-phase given their lifetimes and concentrations.[56] During the measurement periods, the CPF results for $NO_2$ also showed a high probability of high $NO_2$ concentrations in both livestock and urban areas occurring locally, supporting that the high $NO_2$ concentration originated near the study area rather than during long-range transport (Fig. S6†).

Fig. 6 shows the sensitivity results for TN control in livestock and urban areas. The PM mass concentrations decreased linearly as TN decreased in both livestock and urban areas (Fig. 6A and B). In the livestock area, a 50% decrease in the TN resulted in a 50% decrease in the particulate $NO_3^-$ and an approximately 33% decrease in the $PM_{1.0}$ mass concentrations during the

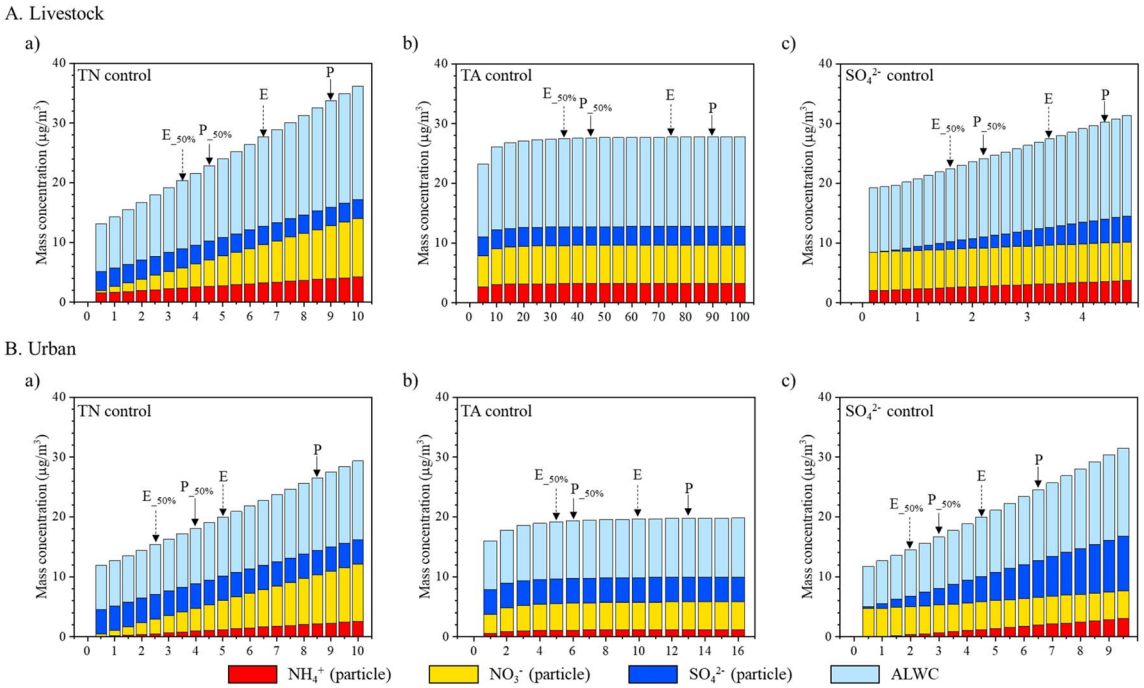


Fig. 6 Thermodynamic ISORROPIA-II model simulations for $SO_4^{2-}$, $NO_3^-$, and $NH_4^+$ (SNA) concentrations and aerosol liquid water content (ALWC) varied by (a) total nitrate (TN), (b) total ammonia (TA) and (c) $SO_4^{2-}$ concentration inputs in (A) livestock and (B) urban areas. "E" indicates the wet particulate matter (PM) mass concentration during entire days and "P" indicates the wet PM mass concentration during pollution days. "$E_{50\%}$" and "$P_{50\%}$" indicate the wet PM mass concentration when TN, TA, and $SO_4^{2-}$ are reduced by up to 50%. The following inputs were used in the model: temperature (livestock: 288.3 K; urban: 288.2 K); relative humidity (livestock: 75%; urban: 64%); and TN, TA, and $SO_4^{2-}$ concentrations (livestock: 6.5, 73.1, and 3.5 μg $m^{-3}$; urban: 4.8, 9.9, and 4.4 μg $m^{-3}$) (Table S1†).

entire period as well as during pollution periods (Fig. 6A). Significant responses in $NO_3^-$ (50%) and $PM_{2.5}$ (~23%) were observed during an entire day in the urban area, but a higher reduction in $NO_3^-$ (50%) and $PM_{2.5}$ (31%) was predicted by a 50% decrease in the TN during pollution days (Fig. 6B). Therefore, to decrease particulate $NO_3^-$ and PM concentrations in both areas, controlling $HNO_3$ is a highly efficient approach.

Second, a sensitivity analysis was performed by controlling TA (Fig. 6). Atmospheric $NH_3$ is generally considered a local contributor because of its short lifetime.[57] As shown in Fig. 6A and B, a 50% decrease in TA did not respond to the $NO_3^-$ and PM concentrations (only ~1% in the livestock site and ~2% in the urban site). An ~87% (livestock) and ~78% (urban) reduction in TA would be required to effectively decrease PM mass concentrations.

Finally, $SO_4^{2-}$ was controlled during the simulation. $SO_4^{2-}$ does not undergo gas-particle partitioning and is favored in the particle-phase because of its low volatility.[4] Reportedly, $SO_2$ can be transported from China to Korea, and therefore, we cannot rule out the possibility of the transported $SO_4^{2-}$.[58]

Illustrated in Fig. 6A and B are the results of $SO_4^{2-}$ control in the two regions. If we assume that $SO_4^{2-}$ is not transported at all to the receptor areas and formed locally by applying to the actual measured concentration of $SO_4^{2-}$ (livestock: 3.5 μg $m^{-3}$ and urban: 4.3 μg $m^{-3}$), only the PM concentration can be found to decrease in the livestock ($PM_{1.0}$: ~20%, $NO_3^-$: ~0.1%, Fig. 6A) and urban areas ($PM_{2.5}$: ~30%, $NO_3^-$: ~0.0%, Fig. 6B) during PM pollution. A similar reduction in PM was observed during the entire period in both areas. However, some $SO_4^{2-}$ may have been transported from outside Korea. A modeling study showed that approximately half of the $SO_4^{2-}$ in $PM_{2.5}$ was transported from China to South Korea during 2012–2016.[58] Accordingly, if we assume that only half of the $SO_4^{2-}$ was locally produced, then a 50% reduction in $SO_4^{2-}$ leads to a reduction in the $PM_{1.0}$ and $PM_{2.5}$ concentrations in the livestock ($PM_{1.0}$: ~12%, $NO_3^-$: ~0.1%, Fig. 6A) and urban areas ($PM_{2.5}$: ~20%, $NO_3^-$: ~0.0%, Fig. 6B) during PM pollution. On an entire day, a 50% decrease in the $SO_4^{2-}$ concentration could lead to a ~13% decrease in PM concentrations and ~0.0% decrease in the particulate $NO_3^-$ concentration in the livestock and urban areas. For $SO_4^{2-}$ control, a linear reduction in the $SO_4^{2-}$ concentration, regardless of whether $SO_4^{2-}$ was transported, resulted in a linear decrease in PM mass concentrations but a non-linear decrease in the particulate $NO_3^-$ concentration.

Additionally, we investigated the effect of TN, TA, and $SO_4^{2-}$ control on the gas-particle partitioning of $HNO_3$ and $NH_3$. Almost ~96% of the TA remains in the gas-phase in a livestock area when the TN, TA, and $SO_4^{2-}$ were reduced (Fig. S7A, S8A, and S9A†); however, a decrease in the TN and $SO_4^{2-}$ led to more evaporation of particulate $NH_4^+$ into more gaseous $NH_3$ in an urban area (Fig. S7B and S9B†). However, the particle-phase of $NO_3^-$ was always the dominant form in both sites (Fig. S7–S9†).

## Conclusions

We monitored $NH_3$, $HNO_3$, and WSII concentrations in $PM_{1.0}$, in a livestock area in Gimje, from June to July 2020 and January to February 2021 to characterize $NO_3^-$ formation. During the study periods, the average concentrations of $NH_3$ and $HNO_3$ were 96.9 and 0.7 ppb, respectively, and the daily average of $PM_{1.0}$ concentration was 20.1 μg $m^{-3}$, with averages of 2.8 μg $m^{-3}$ for $NH_4^+$, 4.8 μg $m^{-3}$ for $NO_3^-$, and 3.5 μg $m^{-3}$ for $SO_4^{2-}$. On pollution days ($PM_{1.0} \geq 20$ μg $m^{-3}$), a remarkable increase in the fraction of $NO_3^-$ in $PM_{1.0}$ and the daily $NH_3$ and $HNO_3$ concentrations was observed, suggesting the critical role of $NH_3$ and $HNO_3$ in $NO_3^-$ formation. The measurements and ISORROPIA-II-simulated results showed that $NO_3^-$ formation in the livestock area was always TN-limited owing to its $NH_3$-rich environment. Recent studies showed that some amount of the water content of organic materials (~30%) could influence the water content and pH of aerosol particles.[36,59] Further studies are needed to confirm the effect of organic materials on aerosol water content. Recent studies reported that VOC reduction would be efficient in reducing $NH_4NO_3$ aerosol in some areas.[60–62] To confirm this, further studies are needed with more measurement datasets.

In comparing the effect of reducing particulate $NO_3^-$ and PM concentrations by controlling TN, TA, and $SO_4^{2-}$ from two different environments (*i.e.*, livestock and urban areas), we found that reducing TN is more effective than reducing TA and $SO_4^{2-}$ in alleviating particulate $NO_3^-$ and PM in both areas. Collectively, our results provide an understanding of the characteristics and formation of $NO_3^-$—the most serious aerosol pollutants in Korea—as well as provide scientific data to develop effective PM reduction policies for livestock and urban areas.

## Author contributions

M. S. designed this study. H. K., J. P., S. G. K. and M. S. conducted measurements and analysed the data. M. S., H. K., K. P. and S. G. K prepared the manuscript.

## Conflicts of interest

There are no conflicts to declare.

## Acknowledgements

This research was supported by the Technology Development Program to Solve Climate Changes of the National Research Foundation (NRF) funded by the Korea government (MSIT) (NRF-2019M1A2A2103956), and by the Fine Particle Research Initiative in East Asia Considering National Differences (FRIEND) Project (NRF-2020M3G1A1114548). We thank Sangmin Oh and Junghyeong Ryu for technical support.

## Notes and references

1 B. B. Booth, N. J. Dunstone, P. R. Halloran, T. Andrews and N. Bellouin, Aerosols implicated as a prime driver of twentieth-century North Atlantic climate variability, *Nature*, 2012, **484**, 228–232, DOI: 10.1016/j.envint.2016.02.003.

2 G. Bhattarai, J. B. Lee, M.-H. Kim, S. Ham, H.-S. So, S. Oh, H.-J. Sim, J.-C. Lee, M. Song and S.-H. Kook, Maternal exposure to fine particulate matter during pregnancy induces progressive senescence of hematopoietic stem cells under preferential impairment of the bone marrow microenvironment and aids development of myeloproliferative disease, *Leukemia*, 2020, **34**, 1481–1484, DOI: 10.3390/ijerph14040440.

3 G. Myhre, D. Shindell and F. M. Breon, *Anthropogenic and natural radiative forcing, in IPCC, Climate Change 2013: The Physical Science Basis, Working Group I Contribution to the IPCC Fifth Assessment Report*, https://www.ipcc.ch/report/ar5/wg1/anthropogenic-and-natural-radiative-forcing/, accessed on 1 April 2022.

4 J. Seinfeld and S. Pandis, *Atmospheric Chemistry and Physics: From Air Pollution to Climate Change*, Wiley, Hoboken, NJ, USA, 3rd edn, 2016, ISBN 978-1-118-94740-1.

5 J. L. Jimenez, M. Canagaratna, N. Donahue, A. Prevot, Q. Zhang, J. H. Kroll, P. F. DeCarlo, J. D. Allan, H. Coe and N. Ng, Evolution of organic aerosols in the atmosphere, *science*, 2009, **326**, 1525–1529, DOI: 10.1126/science.1180353.

6 Z. Cheng, L. Luo, S. Wang, Y. Wang, S. Sharma, H. Shimadera, X. Wang, M. Bressi, R. M. de Miranda and J. Jiang, Status and characteristics of ambient $PM_{2.5}$ pollution in global megacities, *Environ. Int.*, 2016, **89**, 212–221, DOI: 10.1016/j.envint.2016.02.003.

7 Y.-C. Lin, Y.-L. Zhang, M.-Y. Fan and M. Bao, Heterogeneous formation of particulate nitrate under ammonium-rich regimes during the high-$PM_{2.5}$ events in Nanjing, China, *Atmos. Chem. Phys.*, 2020, **20**, 3999–4011, DOI: 10.5194/acp-20-3999-2020.

8 J. Park, E. Kim, S. Oh, H. Kim, S. Kim, Y. P. Kim and M. Song, Contributions of Ammonia to High Concentrations of $PM_{2.5}$ in an Urban Area, *Atmosphere*, 2021, **12**, 1676, DOI: 10.3390/atmos12121676.

9 A. Franchin, D. L. Fibiger, L. Goldberger, E. E. McDuffie, A. Moravek, C. C. Womack, E. T. Crosman, K. S. Docherty, W. P. Dube and S. W. Hoch, Airborne and ground-based observations of ammonium-nitrate-dominated aerosols in a shallow boundary layer during intense winter pollution episodes in northern Utah, *Atmos. Chem. Phys.*, 2018, **18**, 17259–17276, DOI: 10.5194/acp-18-17259-2018.

10 S. S. Brown and J. Stutz, Nighttime radical observations and chemistry, *Chem. Soc. Rev.*, 2012, **41**, 6405–6447, DOI: 10.1039/C2CS35181A.

11 R.-J. Huang, J. Duan, Y. Li, Q. Chen, Y. Chen, M. Tang, L. Yang, H. Ni, C. Lin and W. Xu, Effects of $NH_3$ and alkaline metals on the formation of particulate sulfate and nitrate in wintertime Beijing, *Sci. Total Environ.*, 2020, **717**, 137190, DOI: 10.1016/j.scitotenv.2020.137190.

12 E. E. McDuffie, S. J. Smith, P. O'Rourke, K. Tibrewal, C. Venkataraman, E. A. Marais, B. Zheng, M. Crippa, M. Brauer and R. V. Martin, A global anthropogenic emission inventory of atmospheric pollutants from sector- and fuel-specific sources (1970–2017): an application of the

Community Emissions Data System (CEDS), *Earth Syst. Sci. Data*, 2020, **12**, 3413–3442, DOI: 10.5194/essd-12-3413-2020.

13 P. Oikawa, C. Ge, J. Wang, J. Eberwein, L. Liang, L. Allsman, D. Grantz and G. Jenerette, Unusually high soil nitrogen oxide emissions influence air quality in a high-temperature agricultural region, *Nat. Commun.*, 2015, **6**, 1–10, DOI: 10.1038/ncomms9753.

14 M. Almaraz, E. Bai, C. Wang, J. Trousdell, S. Conley, I. Faloona and B. Z. Houlton, Agriculture is a major source of $NO_x$ pollution in California, *Sci. Adv.*, 2018, **4**, eaao3477, DOI: 10.1126/sciadv.aao3477.

15 X. Lu, X. Ye, M. Zhou, Y. Zhao, H. Weng, H. Kong, K. Li, M. Gao, B. Zheng and J. Lin, The underappreciated role of agricultural soil nitrogen oxide emissions in ozone pollution regulation in North China, *Nat. Commun.*, 2021, **12**, 1–9, DOI: 10.1038/s41467-021-25147-9.

16 M. A. Sutton, S. Reis, S. N. Riddick, U. Dragosits, E. Nemitz, M. R. Theobald, Y. S. Tang, C. F. Braban, M. Vieno and A. J. Dore, Towards a climate-dependent paradigm of ammonia emission and deposition, *Philos. Trans. R. Soc., B*, 2013, **368**, 20130166, DOI: 10.1098/rstb.2013.0166.

17 Z. Zhang, Y. Yan, S. Kong, Q. Deng, S. Qin, L. Yao, T. Zhao and S. Qi, Benefits of refined $NH_3$ emission controls on $PM_{2.5}$ mitigation in Central China, *Sci. Total Environ.*, 2022, **814**, 151957, DOI: 10.1016/j.scitotenv.2021.151957.

18 H. Guo, R. Otjes, P. Schlag, A. Kiendler-Scharr, A. Nenes and R. J. Weber, Effectiveness of ammonia reduction on control of fine particle nitrate, *Atmos. Chem. Phys.*, 2018, **18**, 12241–12256, DOI: 10.5194/acp-18-12241-2018.

19 J. Chen, J. Lu, J. C. Avise, J. A. DaMassa, M. J. Kleeman and A. P. Kaduwela, Seasonal modeling of $PM_{2.5}$ in California's San Joaquin Valley, *Atmos. Environ.*, 2014, **92**, 182–190, DOI: 10.1016/j.atmosenv.2014.04.030.

20 R. Kuprov, D. J. Eatough, T. Cruickshank, N. Olson, P. M. Cropper and J. C. Hansen, Composition and secondary formation of fine particulate matter in the Salt Lake Valley: Winter 2009, *J. Air Waste Manage. Assoc.*, 2014, **64**, 957–969, DOI: 10.1080/10962247.2014.903878.

21 Korean Statistical Information Service (KOSIS), https://kosis.kr, accessed on 1 April 2022.

22 Clean Air Policy Support System (CAPSS). *2017 Korea National Air Pollutants Emission*. 2019, https://airemiss.nier.go.kr, accessed on 1 April 2022.

23 C. Han, S. Kim, Y.-H. Lim, H.-J. Bae and Y.-C. Hong, Spatial and temporal trends of number of deaths attributable to ambient $PM_{2.5}$ in the Korea, *J. Korean Med. Sci.*, 2018, **33**, 1–14, DOI: 10.3346/jkms.2018.33.e193.

24 J.-S. Hwang, Y.-K. Park and C.-H. Won, Runoff characteristics of non-point source pollution in lower reaches of livestock area, *J. Korean Soc. Environ. Eng.*, 2012, **34**, 557–565, DOI: 10.4491/KSEE.2012.34.8.557.

25 ABB, ABB-Los Gatos Research Inc., *Off-Axis Integrated Cavity Output Spectroscopy (OA-ICOS)*, http://www.lgrinc.com/advantages/, accessed on 1 April 2022.

26 E. S. Edgerton, Y.-M. Hsu, E. M. White, M. E. Fenn and M. S. Landis, Ambient concentrations and total deposition of inorganic sulfur, inorganic nitrogen and base cations in the Athabasca Oil Sands Region, *Sci. Total Environ.*, 2020, **706**, 134864, DOI: 10.1016/j.scitotenv.2019.134864.

27 M. Sung, J. Park, J. Lim, H. Park and S. Cho, A long term trend of gaseous and particulate acid/base species and effects of ammonia reduction on nitrate contained in $PM_{2.5}$, 2009∼ 2018, *J. Korean Soc. Atmos*, 2020, **36**, 249–261, DOI: 10.5572/KOSAE.2020.36.2.249.

28 C. J. Tsai, C. H. Huang and H. H. Lu, Adsorption capacity of a nylon filter of filter pack system for HCl and $HNO_3$ gases, *Sep. Sci. Technol.*, 2005, **39**, 629–643, DOI: 10.1081/SS-120027998.

29 W. Nie, T. Wang, X. Gao, R. K. Pathak, X. Wang, R. Gao, Q. Zhang, L. Yang and W. Wang, Comparison among filter-based, impactor-based and continuous techniques for measuring atmospheric fine sulfate and nitrate, *Atmos. Environ.*, 2010, **44**, 4396–4403, DOI: 10.1016/j.atmosenv.2010.07.047.

30 Environmental Protection Agency (EPA), http://www.epa.gov/aqs, accessed on 1 April 2022.

31 S. Oh, S.-G. Kim, J. B. Lee, J. Park, J.-B. Jee, S.-W. Hong, K.-S. Kwon and M. Song, Spatial distributions of atmospheric ammonia in a rural area in south Korea and the associated impact on a nearby urban area, *Atmosphere*, 2021, **12**, 1411, DOI: 10.3390/atmos12111411.

32 ECOTECH, *Environmental monitoring, Serinus 40 oxides of Nitrogen analyzer, user manual, version 3.5*, https://www.ecotech.com/, accessed on 1 April 2022.

33 Korea Meteorological Administration (KMA), https://data.kma.go.kr/cmmn/main.do, accessed on 1 April 2022.

34 ISORROPIA, *version 2.1*, http://nenes.eas.gatech.edu/ISORROPIA, accessed on 1 April 2022.

35 C. Fountoukis and A. Nenes, ISORROPIA II: a computationally efficient thermodynamic equilibrium model for $K^+$–$Ca^{2+}$–$Mg^{2+}$–$NH_4^+$–$Na^+$–$SO_4^{2-}$–$NO_3^-$–$Cl^-$–$H_2O$ aerosols, *Atmos. Chem. Phys.*, 2007, **7**, 4639–4659, DOI: 10.5194/acp-7-4639-2007.

36 X. Jin, Y. Wang, Z. Li, F. Zhang, W. Xu, Y. Sun, X. Fan, G. Chen, H. Wu and J. Ren, Significant contribution of organics to aerosol liquid water content in winter in Beijing, China, *Atmos. Chem. Phys.*, 2020, **20**, 901–914, DOI: 10.5194/acp-20-901-2020.

37 Y. B. Lim, J. Seo, J. Y. Kim, Y. P. Kim and H. C. Jin, Local formation of sulfates contributes to the urban haze with regional transport origin, *Environ. Res. Lett.*, 2020, **15**, 084034, DOI: 10.1088/1748-9326/ab83aa.

38 W. Li, X. Teng, X. Chen, L. Liu, L. Xu, J. Zhang, Y. Wang, Y. Zhang and Z. Shi, Organic coating reduces hygroscopic growth of phase-separated aerosol particles, *Environ. Sci. Technol.*, 2021, **55**, 16339–16346, DOI: 10.1021/acs.est.1c05901.

39 J. Sun, L. Liu, L. Xu, Y. Wang, Z. Wu, M. Hu, Z. Shi, Y. Li, X. Zhang and J. Chen, Key role of nitrate in phase transitions of urban particles: implications of important reactive surfaces for secondary aerosol formation, *J. Geophys. Res.: Atmos.*, 2018, **123**, 1234–1243, DOI: 10.1002/2017JD027264.

40 J. Seo, Y. B. Lim, D. Youn, J. Y. Kim and H. C. Jin, Synergistic enhancement of urban haze by nitrate uptake into transported hygroscopic particles in the Asian continental outflow, *Atmos. Chem. Phys.*, 2020, **20**, 7575–7594, DOI: 10.5194/acp-20-7575-2020.

41 W. Xu, Q. Wu, X. Liu, A. Tang, A. J. Dore and M. R. Heal, Characteristics of ammonia, acid gases, and $PM_{2.5}$ for three typical land-use types in the North China Plain, *Environ. Sci. Pollut. Res.*, 2016, **23**, 1158–1172, DOI: 10.1007/s11356-015-5648-3.

42 P. Acharja, K. Ali, D. K. Trivedi, P. Safai, S. Ghude, T. Prabhakaran and M. Rajeevan, Characterization of atmospheric trace gases and water soluble inorganic chemical ions of $PM_1$ and $PM_{2.5}$ at Indira Gandhi International Airport, New Delhi during 2017–18 winter, *Sci. Total Environ.*, 2020, **729**, 138800, DOI: 10.1016/j.scitotenv.2020.138800.

43 Z. Meng, X. Xu, W. Lin, B. Ge, Y. Xie, B. Song, S. Jia, R. Zhang, W. Peng and Y. Wang, Role of ambient ammonia in particulate ammonium formation at a rural site in the North China Plain, *Atmos. Chem. Phys.*, 2018, **18**, 167–184, DOI: 10.5194/acp-18-167-2018.

44 J. Bahino, V. Yoboué, C. Galy-Lacaux, M. Adon, A. Akpo, S. Keita, C. Liousse, E. Gardrat, C. Chiron and M. Ossohou, A pilot study of gaseous pollutants' measurement ($NO_2$, $SO_2$, $NH_3$, $HNO_3$ and $O_3$) in Abidjan, Côte d'Ivoire: contribution to an overview of gaseous pollution in African cities, *Atmos. Chem. Phys.*, 2018, **18**, 5173–5198, DOI: 10.5194/acp-18-5173-2018.

45 Y. Li, F. M. Schwandner, H. J. Sewell, A. Zivkovich, M. Tigges, S. Raja, S. Holcomb, J. V. Molenar, L. Sherman and C. Archuleta, Observations of ammonia, nitric acid, and fine particles in a rural gas production region, *Atmos. Environ.*, 2014, **83**, 80–89, DOI: 10.1016/j.atmosenv.2013.10.007.

46 M. Mozurkewich, The dissociation constant of ammonium nitrate and its dependence on temperature, relative humidity and particle size, *Atmos. Environ., Part A*, 1993, **27**, 261–270, DOI: 10.1016/0960-1686(93)90356-4.

47 J. Neuman, J. Nowak, C. Brock, M. Trainer, F. Fehsenfeld, J. Holloway, G. Hübler, P. Hudson, D. Murphy and D. Nicks Jr, Variability in ammonium nitrate formation and nitric acid depletion with altitude and location over California, *J. Geophys. Res.: Atmos.*, 2003, **108**, 4557, DOI: 10.1029/2003JD003616.

48 Y. Chang, Z. Zou, Y. Zhang, C. Deng, J. Hu, Z. Shi, A. J. Dore and J. L. Collett Jr, Assessing contributions of agricultural and nonagricultural emissions to atmospheric ammonia in a Chinese megacity, *Environ. Sci. Technol.*, 2019, **53**, 1822–1833, DOI: 10.1021/acs.est.8b05984.

49 C. Loftus, M. Yost, P. Sampson, E. Torres, G. Arias, V. B. Vasquez, K. Hartin, J. Armstrong, M. Tchong-French and S. Vedal, Ambient ammonia exposures in an agricultural community and pediatric asthma morbidity, *Epidemiology*, 2015, **26**, 794, DOI: 10.1097/EDE.0000000000000368.

50 Y. Sun, Q. Jiang, Z. Wang, P. Fu, J. Li, T. Yang and Y. Yin, Investigation of the sources and evolution processes of severe haze pollution in Beijing in January 2013, *J. Geophys. Res.: Atmos.*, 2014, **119**, 4380–4398, DOI: 10.1002/2014JD021641.

51 H. Zhang, S. Cheng, X. Wang, S. Yao and F. Zhu, Continuous monitoring, compositions analysis and the implication of regional transport for submicron and fine aerosols in Beijing, China, *Atmos. Environ.*, 2018, **195**, 30–45, DOI: 10.1016/j.atmosenv.2018.09.043.

52 G. Zheng, H. Su, S. Wang, M. O. Andreae, U. Pöschl and Y. Cheng, Multiphase buffer theory explains contrasts in atmospheric aerosol acidity, *Science*, 2020, **369**, 1374–1377, DOI: 10.1126/science.aba3719.

53 M. Tian, H. Wang, Y. Chen, F. Yang, X. Zhang, Q. Zou, R. Zhang, Y. Ma and K. He, Characteristics of aerosol pollution during heavy haze events in Suzhou, China, *Atmos. Chem. Phys.*, 2016, **16**, 7357–7371, DOI: 10.5194/acp-16-7357-2016.

54 C. Fountoukis, A. Nenes, A. Sullivan, R. Weber, T. V. Reken, M. Fischer, E. Matías, M. Moya, D. Farmer and R. Cohen, Thermodynamic characterization of Mexico City aerosol during MILAGRO 2006, *Atmos. Chem. Phys.*, 2009, **9**, 2141–2156, DOI: 10.5194/acp-9-2141-2009.

55 Z. Xu, M. Liu, M. Zhang, Y. Song, S. Wang, L. Zhang, T. Xu, T. Wang, C. Yan and T. Zhou, High efficiency of livestock ammonia emission controls in alleviating particulate nitrate during a severe winter haze episode in northern China, *Atmos. Chem. Phys.*, 2019, **19**, 5605–5613, DOI: 10.5194/acp-19-5605-2019.

56 A. H. Souri, Y. Choi, W. Jeon, J. H. Woo, Q. Zhang and J. i. Kurokawa, Remote sensing evidence of decadal changes in major tropospheric ozone precursors over East Asia, *J. Geophys. Res.: Atmos.*, 2017, **122**, 2474–2492, DOI: 10.1002/2016JD025663.

57 C. Hendriks, R. Kranenburg, J. Kuenen, B. Van den Bril, V. Verguts and M. Schaap, Ammonia emission time profiles based on manure transport data improve ammonia modelling across north western Europe, *Atmos. Environ.*, 2016, **131**, 83–96, DOI: 10.1016/j.atmosenv.2016.01.043.

58 C. Bae, B.-U. Kim, H. C. Kim, C. Yoo and S. Kim, Long-range transport influence on key chemical components of $PM_{2.5}$ in the Seoul metropolitan area, South Korea, during the years 2012–2016, *Atmosphere*, 2019, **11**, 48, DOI: 10.3390/atmos11010048.

59 S. Lv, F. Wang, C. Wu, Y. Chen, S. Liu, S. Zhang, D. Li, W. Du, F. Zhang and H. Wang, Gas-to-Aerosol Phase Partitioning of Atmospheric Water-Soluble Organic Compounds at a Rural Site in China: An Enhancing Effect of $NH_3$ on SOA Formation, *Environ. Sci. Technol.*, 2022, **56**, 3915–3924, DOI: 10.1021/acs.est.1c06855.

60 M. Li, Z. Zhang, Q. Yao, T. Wang, M. Xie, S. Li, B. Zhuang and Y. Han, Nonlinear responses of particulate nitrate to $NO_x$ emission controls in the megalopolises of China, *Atmos. Chem. Phys.*, 2021, **21**, 15135–15152, DOI: 10.5194/acp-21-15135-2021.

61 X. Fu, T. Wang, J. Gao, P. Wang, Y. Liu, S. Wang, B. Zhao and L. Xue, Persistent heavy winter nitrate pollution driven by increased photochemical oxidants in northern China, *Environ. Sci. Technol.*, 2020, **54**, 3881–3889, DOI: **10.1021/acs.est.9b07248**.

62 C. Womack, E. McDuffie, P. Edwards, R. Bares, J. de Gouw, K. Docherty, W. Dubé, D. Fibiger, A. Franchin and J. Gilman, An odd oxygen framework for wintertime ammonium nitrate aerosol pollution in urban areas: $NO_x$ and VOC control as mitigation strategies, *Geophys. Res. Lett.*, 2019, **46**, 4971–4979, DOI: **10.1029/2019GL082028**.